Technical Report
TR-23-21
November 2023

Glacial erosion rates at Forsmark derived from Terrestrial Cosmogenic Nuclides – additional results

Adrian M Hall
Jakob Heyman
Andy Hein

SVENSK KÄRNBRÄNSLEHANTERING AB

SWEDISH NUCLEAR FUEL
AND WASTE MANAGEMENT CO

Box 3091, SE-169 03 Solna
Phone +46 8 459 84 00
skb.se

SVENSK KÄRNBRÄNSLEHANTERING

ISSN 1404-0344
SKB TR-23-21
ID 2012882
November 2023

Glacial erosion rates at Forsmark derived from Terrestrial Cosmogenic Nuclides – additional results

Adrian M Hall
Institute of Geography, University of Edinburgh

Jakob Heyman
Department of Earth Sciences, University of Gothenburg

Andy Hein
Institute of Geography, University of Edinburgh

Keywords: Glacial erosion, Terrestrial Cosmogenic Nuclides, Abrasion, Block removal, Rock fracture.

This report concerns a study which was conducted for Svensk Kärnbränslehantering AB (SKB). The conclusions and viewpoints presented in the report are those of the authors. SKB may draw modified conclusions, based on additional literature sources and/or expert opinions.

This report is published on www.skb.se

© 2023 Svensk Kärnbränslehantering AB

Abstract

This report presents results for a set of Terrestrial Cosmogenic Nuclide (TCN) samples taken from four sites close to the present shoreline at Forsmark. The sampling was undertaken to support a new study of glacial micro-forms and erosion rates during deglaciation. The samples extend the previously reported TCN dataset for the wider Forsmark region.

The sample set includes five paired samples from the top and base of rock steps and one new surface sample. Additionally, one new short (2.3 m) drill profile was obtained from Wave Rock in massive granite gneiss that previous work had shown to hold large TCN inventories. Glacial erosion was simulated based on the depth and time dependent production of ^{10}Be and ^{26}Al for a range of scenarios that include different start times and erosion modes yielding various production rates over time for the individual samples. The glacial erosion estimates reported here conform with previous estimates of depths and rates of glacial erosion for the Forsmark region but tend towards the lower end of previous estimates. For the depth profile, simulations starting at 624 thousand years ago (ka BP) yield constant glacial erosion rates of 0–25 mm/ka for the full set of samples at Wave Rock. Results from four of the step samples are consistent with formation of steps by block removal (‘plucking/quarrying’) during the last ice-covered period (35.4–10.8 ka BP). Erosion estimates for the last ice-covered period were compared between i) abraded surfaces at the summit of Wave Rock and ii) surfaces with micro-erosion forms that indicate combined abrasion and block removal at three other lower elevation sites in the vicinity of Wave Rock and at five other coastal sites. Estimated abrasion depths for the last ice cover period are low (23–46 cm) compared to combined abrasion and block removal depths (117–215 cm), showing that combined abrasion and block removal operated approximately four times faster than abrasion alone.

Sammanfattning

Denna rapport presenterar resultat för en uppsättning prov av terrestra kosmogena nuklider (TCN) tagna från fyra platser nära den nuvarande strandlinjen vid Forsmark. Provtagningen gjordes för att stödja en ny studie av glaciala mikroformer och erosionshastigheter under den senaste deglaciationen. Proverna kompletterar tidigare rapporterade TCN-värden för Forsmarksregionen.

Provsetet innehåller fem parade prover från toppen och basen hos topografiska steg samt ett nytt ytprov. Dessutom erhölls en ny kort (2,3 m) borrprofil från platsen Wave Rock i en massiv granitgnejs vilken tidigare har visats innehålla ett stort TCN-inventarie. Glacial erosion simulerades baserat på den djup- och tidsberoende produktionen av ^{10}Be och ^{26}Al för en rad scenarier som tar hänsyn till olika starttider och erosionssätt (vilket ger olika produktionshastigheter över tid för de individuella proverna). Uppskattningarna av den glaciala erosionen som redovisas här överensstämmer med tidigare uppskattningar från regionen men tenderar att vara något lägre än tidigare. För djupprofilen ger simuleringar som börjar för 624 tusen år sedan (ka BP) konstanta glaciala erosionshastigheter på 0–25 mm/ka för hela uppsättningen av prover från Wave Rock. Resultaten från fyra av proverna från de topografiska stegen överensstämmer med att stegen bildats genom plockning av block någon gång under den senaste istäckta perioden (35.4–10.8 ka BP). Erosionsuppskattningar för den senaste istäckta perioden jämfördes mellan i) slipade ytor på toppen av Wave Rock och ii) ytor med mikro-erosionsformer som visar på både slipning och plockning vid tre andra lokaler på lägre höjd i närheten av Wave Rock samt vid fem andra kustnära platser. De uppskattade erosionsdjupen orsakade av enbart slipning under den senaste istäckta perioden är låga (23–46 cm) i jämförelse med djupen från en kombination av slipning och plockning (117–215 cm). Detta visar att erosionshastigheten vid kombinerad slipning och plockning var ungefär fyra gånger så hög som erosionshastigheten vid enbart slipning.

Contents

1 Introduction

Glacial erosion is the process by which glaciers and ice sheets modify and shape the Earth's surface by removing rock or sediment at the glacier bed. During future glaciations at Forsmark, this process will lead to a lowering of the bedrock surface above SKB's planned and existing nuclear waste repositories, thereby changing i) groundwater flow and radionuclide transport times and ii) enhancing the risk of freezing at repository depth during subsequent periods of permafrost in the area. Based on previous investigations (Hall et al. 2019), SKB has concluded that glacial erosion, together with other erosion processes and weathering, will contribute to a lowering of the surface at Forsmark by less 1 m over the next 100 000 years, and likely 5–28 m over the next 1 million years (SKB 2020, Section 3.5).

Previous investigations have examined the impact of past glacial erosion on the Precambrian basement gneiss surfaces at Forsmark (Hall et al. 2019). An important part of these assessments involved the use of Terrestrial Cosmogenic Nuclides (TCNs) from 32 surface bedrock samples along a 50 km long transect SW of Forsmark (Figure 5-2 in Hall et al. 2019). The aim was to estimate depths and rates of glacial erosion through the last and earlier glacial cycles and to estimate erosion rates for possible future glacial cycles over the next 100 thousand years (ka) and 1 million years (Ma) (Hall et al. 2019). A more recent and separate study aims to better understand the specific contribution of block removal to glacial erosion budgets during phases of ice retreat (Krabbendam et al. 2023). This micro-erosion study focussed on detailed surveys of micro- and meso-scale glacial erosion forms on gneiss surfaces exposed at 4 sites on the present coastline near Forsmark: Lilla Sandgrund, Stora Asphällan, Stånggrundet and Klubbudden (Figure 1-1). The methodology used involved (i) the mapping of precursor abraded rock surfaces, (ii) projection of these surfaces to reconstruct the earlier forms that existed before late block removal, and (iii) calculation of volume of rock removed between the reconstructed surfaces and the present rock surface. Abraded surfaces are interpreted to have been eroded by abrasion only, without earlier block removal.

To better constrain erosion rates in the Forsmark area, a further set of TCN samples were taken from 4 sites near Forsmark: Lilla Sandgrund, Gunnarsbo, Mohägnaden and Wave Rock (Figure 1-1). These included 5 paired sets of step samples from sites where block removal had formed small leeside and flank cliffs to small roches moutonnées. Comparisons of TCN inventories for top and bottom step surfaces provide improved constraints on background glacial erosion rates during the last glaciation (35.4–10.8 ka before present (BP)) and over multiple glaciations potentially extending back to 0.6 Ma. Additionally, one short (2.3 m) drill core was obtained at Wave Rock from a summit surface in a tonalite gneiss. Existing data at Wave Rock indicate that TCN inventories are the largest known in the Forsmark area, consistent with slow erosion (Hall et al. 2019). The summit surface has widely spaced fractures and is dominated by micro-forms formed by sustained abrasion; new samples have potential to constrain long-term abrasion rates. Existing and new TCN data allow comparisons between sites at the present coastline and i) previous estimates of glacial erosion over the last ~1 Ma based on geomorphological and TCN evidence (Hall et al. 2019), and ii) for the last deglaciation based on depths of glacial ripping (Hall et al. 2020), and iii) help to constrain background erosion rates on precursor rock surfaces in the micro-erosion study.

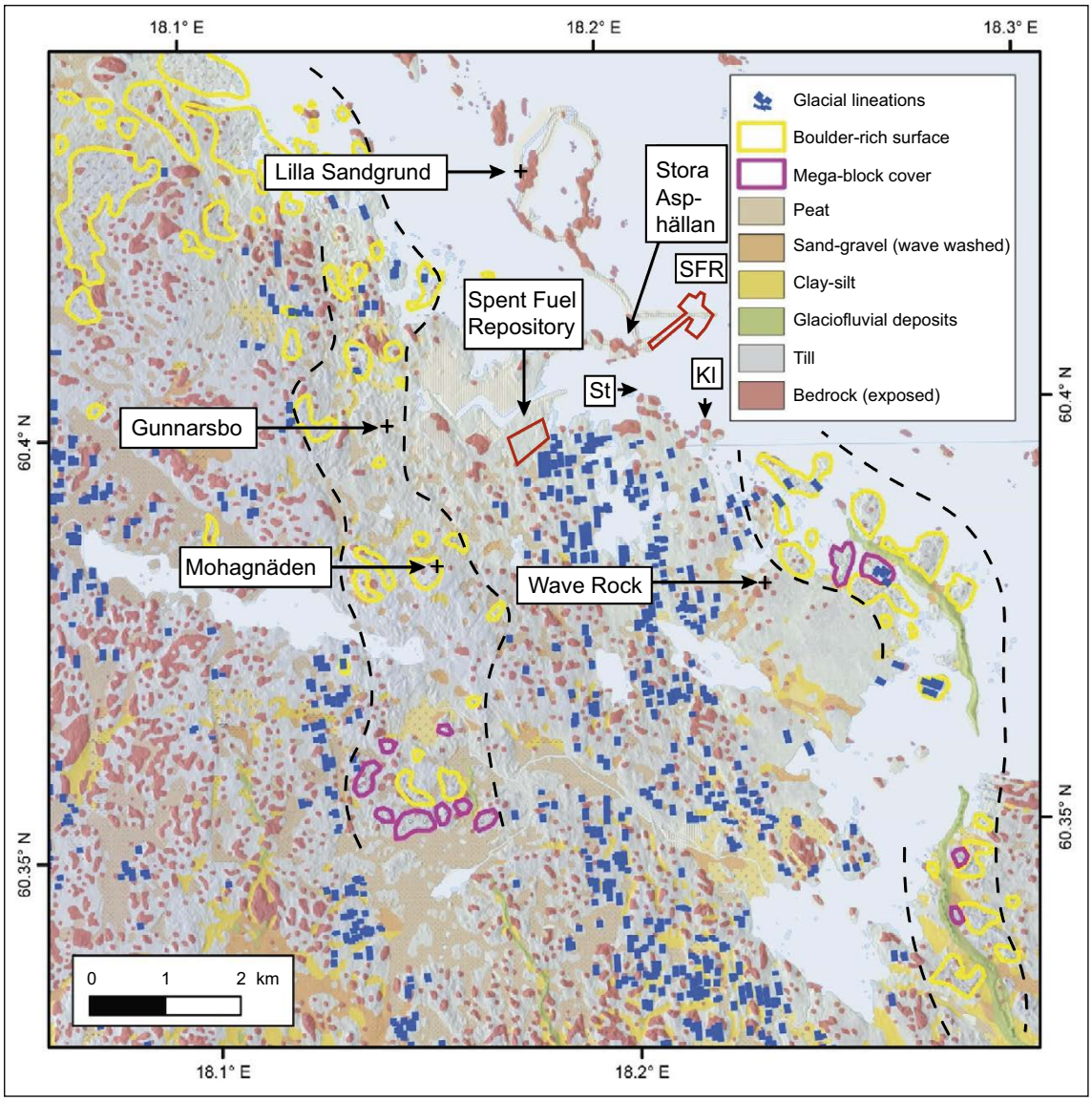

Figure 1-1. *Locations of Terrestrial Cosmogenic Nuclide samples for the present study collected in 2019. The dashed black lines delimit potential meltwater corridors. The red lines delimit the SFR (SKB's repository for short-lived radioactive waste) and the Spent Fuel Repository (SKB's planned repository for spent nuclear fuel). Background geomorphological map from Figure 4-27 in Hall et al. (2019). The dashed black lines are the inferred boundaries of subglacial meltwater corridors. Kl Klubbudden. St Stånggrundet.*

2 Method

2.1 Sampling

We collected new samples for cosmogenic nuclide analysis in 2019 from four sites in the vicinity of Forsmark at elevations of 1–20 m a.s.l. (Figure 2-1). Sample sites at Gunnarsbo and Mohägnaden lie in terrain with boulder spreads interpreted as products of glacial ripping along potential subglacial meltwater corridors (Krabbendam et al. 2022). Lilla Sandgrund and Wave Rock lack boulder spreads and lie outside these corridors (Figure 1-1).

Paired TCN samples have been used previously to constrain the timing of glacial removal of tor blocks (Phillips et al. 2006, Margreth et al. 2014). Here, we use paired samples from rock steps to determine the timing of block removal. Paired samples were collected from three bedrock steps at Gunnarsbo, Mohägnaden, and Lilla Sandgrund, with an upper sample from the top of the bedrock step and a lower sample below or at the edge of a bedrock step (Figure 2-1). All upper samples were from surfaces that showed evidence for sustained glacial abrasion, such as striae, but which may also have lost mass by block removal. One additional surface bedrock sample was collected at Lilla Sandgrund from close to one of the bedrock steps. At Wave Rock (Figure 2-2), existing TCN data was extended by adding two further paired step samples. A 2.3 m deep bedrock core was also drilled from the abraded summit surface adjacent to the two bedrock step sample points (Figure 2-3). The hand-held diamond drill yielded 41 mm diameter cores.

Previously, in 2016/2017, five rock surfaces were sampled from Lilla Sandgrund and another three rock surfaces were sampled from Stånggrundet but samples did not yield reliable TCN data because the quartz grains were too small.

2.2 Sample preparation and analysis

The samples were chemically prepared as ^{10}Be and ^{26}Al Accelerator Mass Spectrometry (AMS) targets at the University of Edinburgh's Cosmogenic Nuclide Laboratory and were measured at the AMS facility at the Scottish Universities Environmental Research Centre (SUERC; East Kilbride, UK). The rock samples were crushed and sieved to obtain the 250–710 µm fraction. Cosmogenic ^{10}Be and ^{26}Al were selectively extracted from 20–22 g of the quartz component of the whole-rock sample following established methods (Kohl and Nishiizumi 1992, Bierman et al. 2002). Process blanks (n = 4 × Be; 4 × Al) were spiked with 250 µg ^{9}Be carrier (Scharlau Be carrier, 1 000 mg/l, density 1.02 g/ml) and 1.5 mg ^{27}Al carrier (SpexCertiPrep Al carrier, 1 000 ppm). Samples were spiked with 250 µg ^{9}Be carrier and up to 1.5 mg ^{27}Al carrier (the amount varied with the native Al-content). ^{10}Be/^{9}Be and ^{26}Al/^{27}Al measurements are normalised to the NIST SRM-4325 Be standard material with a revised (Nishiizumi et al. 2007) nominal ^{10}Be/^{9}Be of 2.79×10^{-11}, and the Purdue Z92-0222 Al standard material with a nominal ^{26}Al/^{27}Al of 4.11×10^{-11}, which agrees with the Al standard material of Nishiizumi (2004). SUERC ^{10}Be-AMS is insensitive to ^{10}B interference (Xu et al. 2013) and the interferences to ^{26}Al detection are well characterized (Xu et al. 2014).

2.3 Sample site descriptions

The contexts of the new 2019 sample sites are described below. TCN sample sites from 2016–2018 were described in Hall et al. (2019). Fracturing and surface form at several coastal sites sampled in that campaign are also described below.

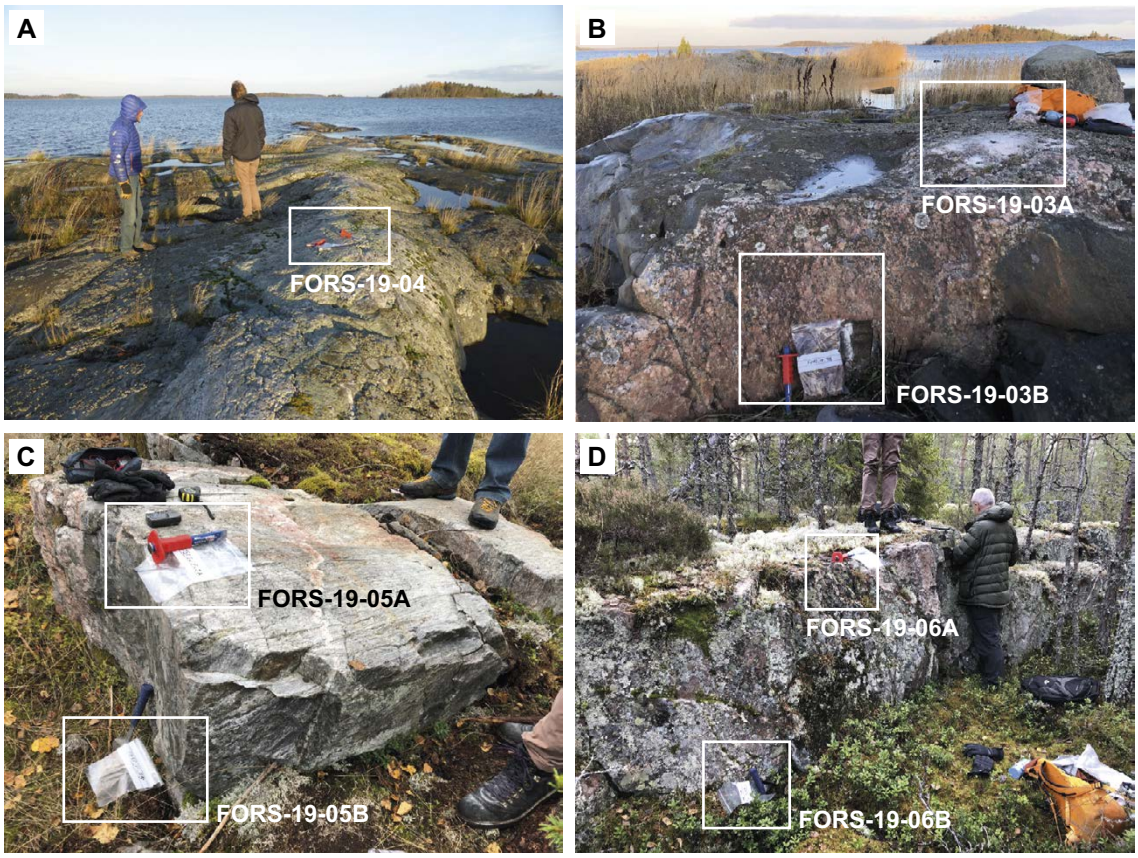

Figure 2-1. *Surface and step samples. A. Lilla Sandgrund surface sample (FORS-19-04). B. Lilla Sandgrund step samples (FORS-19-03). C. Gunnarsbo step samples (FORS-19-05). D. Mohägnaden step samples (FORS-19-06).*

2.3.1 Lilla Sandgrund

A 1 m high, smooth asymmetric ridge is developed in a quartz-rich granitic pegmatite dyke on the shoreline at Lilla Sandgrund (Figure 2-1A). The exposed surface of the dyke has polished phenocrysts but has a high micro-roughness due to the removal of rock chips typical of glacial microforms in this rock type. A surface sample (FORS-19-04) was taken with a hammer and chisel by removing quartz chips over an area of 20 × 10 cm to a depth of 4 cm.

A low (~0.5 m) roche moutonnée lies 50 m to the SE (Figure 2-1B). Its lee-side cliff exposes a quartz rich pegmatite vein. A subhorizontal fracture follows the contact with the underlying amphibolite at ~35–60 cm depth. In the immediate vicinity of the roche moutonnée dilated (4–10 mm) subhorizontal fractures and slightly disrupted surfaces are consistent with shallow, lee side hydraulic jacking under conditions of localised groundwater overpressure.

A surface sample (FORS-19-03A) was taken with a hammer and chisel by removing quartz chips from the pegmatite vein over an area of 20 × 30 cm to a depth of 1–1.5 cm. A lower sample (FORS-19-03B) from the base of the step is at a depth 0.65 m below FORS-19-03A. The top of the lower sample flake was 20 cm from the base of the cliff.

2.3.2 Gunnarsbo

Gunnarsbo is a locality with an extensive boulder spread interpreted as a product of glacial ripping within which lie a few, small rock outcrops (Hall et al. 2020, Krabbendam et al. 2022). The orientations of gneiss foliation and striae at the sample site are parallel to those measured in the surroundings and indicate that the rock at the sample site is *in situ*.

A paired step sample was taken by hammer and chisel (Figure 2-1C). The top sample (FORS-19-05A) is 7 cm deep and comes from the top edge of a lee-side cliff. The base sample (FORS-19-05B) is 15 cm thick, with the base of the step 70 cm below the top edge.

2.3.3 Mohägnaden

This hill has a large antenna tower and was previously informally named as Antenna View (Hall et al. 2019). The correct local name for this hill is Mohägnaden. The amphibolite hilltop shows extensive abraded and plucked surfaces with bounding cliffs from which many blocks have been removed to form boulder spreads on the stoss, flank and lee slopes.

A paired step sample was taken by hammer and chisel from a zone of quartz-rich gneiss along a 1.35 m high flank cliff (Figure 2-1D). The sample edge is oriented N–S and shows unabraded edges to projecting rock blocks that are consisting with removal of rock from the edge at a late stage of deglaciation. FORS-19-06A comes from the top edge of the cliff. FORS-19-06B comes from the base of the step at 60 cm depth, with a 15 cm depth range.

2.3.4 Wave Rock

Wave Rock is an informal name given previously (Hall et al. 2019) to a low rock hill intermediate in form between a whaleback and roche moutonnée with a summit at 11 m a.s.l. south–west of Tixelfjärden (Figures 2-2 and 2-3). The hill summit is developed in unusually massive porphyritic tonalitic gneiss with a wide spacing of vertical fractures that locally exceeds 10 m. In the surroundings, the dominant rock type is a grey, medium-grained and equigranular metatonalite with segregations and veins of pegmatite. The metatonalite shows a conspicuous, linear grain-shape fabric oriented 140°/30° and is also foliated (L > S tectonite) (Stephens 2010). The dominant trends for lineament orientations seen in Digital Elevation Models are NW–SE and NE−SW, indicating that vertical fracture sets lie oblique to ice flow from the north. On the summit surface, the dominant fracture set is oriented 145–325° (see Figure 4-39 in Hall et al. 2019). Subhorizontal fractures with > 1.4 m vertical spacing are exposed in places on the flanks of the summit outcrop, away from the mapped summit area, and likely control the overall convex hill form. No evidence of glacial ripping is seen at Wave Rock but disrupted terrain with boulder spreads is found < 0.5 km NE of the site and extends towards Tixelfjärden (Figure 2-2C).

Detailed mapping of fractures has been carried out from a 20 m^2 area around the Wave Rock summit sample site (Hall et al. 2019). This part of the outcrop is formed in tonalitic gneiss that varies from fine-grained (mean feldspar crystal length of 0.8 mm; 1 σ (i.e. 1 standard deviation) = 0.3 mm) to pegmatitic (mean feldspar length of 10.4 mm; 1 σ = 4.9 mm). Pegmatites occur as veins and appear on the outcrop surface as lenses. Sub-vertical fractures track the pegmatite veins, and the cosmogenic nuclide sample sites are in this zone of pegmatites. The mean spacing of the mapped sub-vertical fractures is 1.1 m, which is the widest recorded for any of the 12 sample outcrops at Forsmark measured by the same method. Fracture spacing of long, continuous vertical fractures measured using a different method along survey lines, however, is much wider at 5.5 m (Section 4.3.4 in Hall et al. 2019).

The gently undulating summit surface of the hill has < 1.5 m relief over an area of ~6 000 m^2. The summit surface of Wave Rock lacks typical micro- to macro-forms formed by processes other than abrasion. Instead, its smooth surfaces, rounded step edges, chock marks, and glacially polished phenocrysts together indicate the sustained operation of processes of glacial abrasion during the last phase of glacial erosion. At FORS-19-08 the sub-horizontal fracture spacing is > 1.14 m. The removal of small blocks by glacial erosion is suppressed across the summit surface of Wave Rock by wide fracture spacing, although 1–2 cm thick plates are observed to have spalled from southern parts of the summit surface. Vertical fractures remain tight. Hence, the upper part of the rock step at the Wave and the wider summit surface at Wave Rock may have been subject to abrasion only throughout the last glaciation. The preservation of polished surfaces indicates that weathering of the rock surface since its emergence in the late Holocene from 1.8 ka onwards has been very limited. Most edges to fractures are well-rounded and there are only occasional, widely spaced, centimetre deep, shallow sockets.

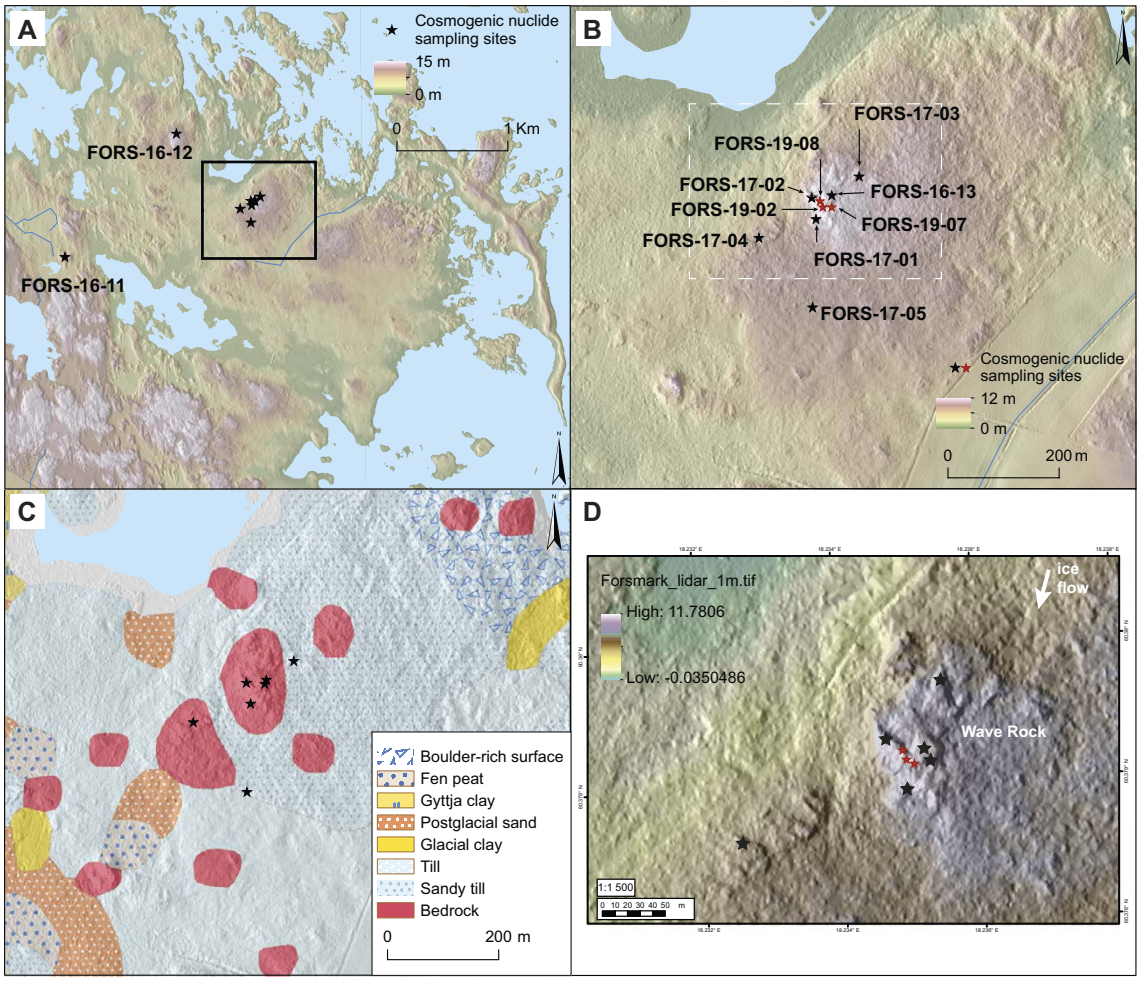

Figure 2-2. *Wave Rock with TCN sample sites. Adapted from Figure 4-30 in Hall et al. (2019). A. DEM showing the topographic setting of Wave Rock. B. Locations of TCN sample sites.. C. SGU Map extract showing rock outcrops and the area with high surface boulder concentrations to the north–east. D. Detail of Wave Rock. Location shown as dashed white line in B.*

Samples FORS-16-13, 17-01, and 17-02 (reported in Hall et al. 2019), and 19-07A and 19-08A come from the summit surface (Figure 2-2). A 2.30 m long core (FORS 19-02) was also recovered from the summit surface with material sufficient for a cosmogenic nuclide depth profile. The drill site is 16 m south of sample site FORS-16-13 and 32 m east of FORS-17-02 (Figure 2-2). The sample surface is smooth and abraded, with planed quartz and feldspar megacrysts, and closed vertical fractures spaced at 3.5 m.

The flanks of the hill show 0.5–2 m high rock steps with sockets where rock blocks have been removed by plucking. Two step samples (FORS-19-07 and -08) come from this setting.

The Wave is a distinctive curved rock step (Figure 2-3A–C). One step sample site (FORS 19-08) lies 12 m west of the depth profile sample site (FORS-19-02). The top sample (FORS-19-08A) is a short (6 cm) drill core taken from 3.8 m south from the base sample (19-08B); the lower sample (B) was taken by chisel at 1.14 m below. The upper 0.74 m of The Wave is abraded and highly rounded, with many crescentic fractures (Figure 2-3C inset). The lower 0.4 m of the step is not abraded and lacks crescentic fractures; it is likely to have lost small blocks during the last glaciation.

A second rock step lies 8 m east of the depth profile sample site (Figure 2-2). The top sample surface is abraded and smooth (FORS-19-07A); the lower sample is 85 cm lower and from the base of the step (FORS-19-07B) (Figure 2-3D). The edges of the abraded top of the cliff are sharp to slightly rounded, and the edges and bases of sockets from where one or more blocks have been removed also show little abrasion. This angularity is consistent with block removal by plucking late in the last glaciation.

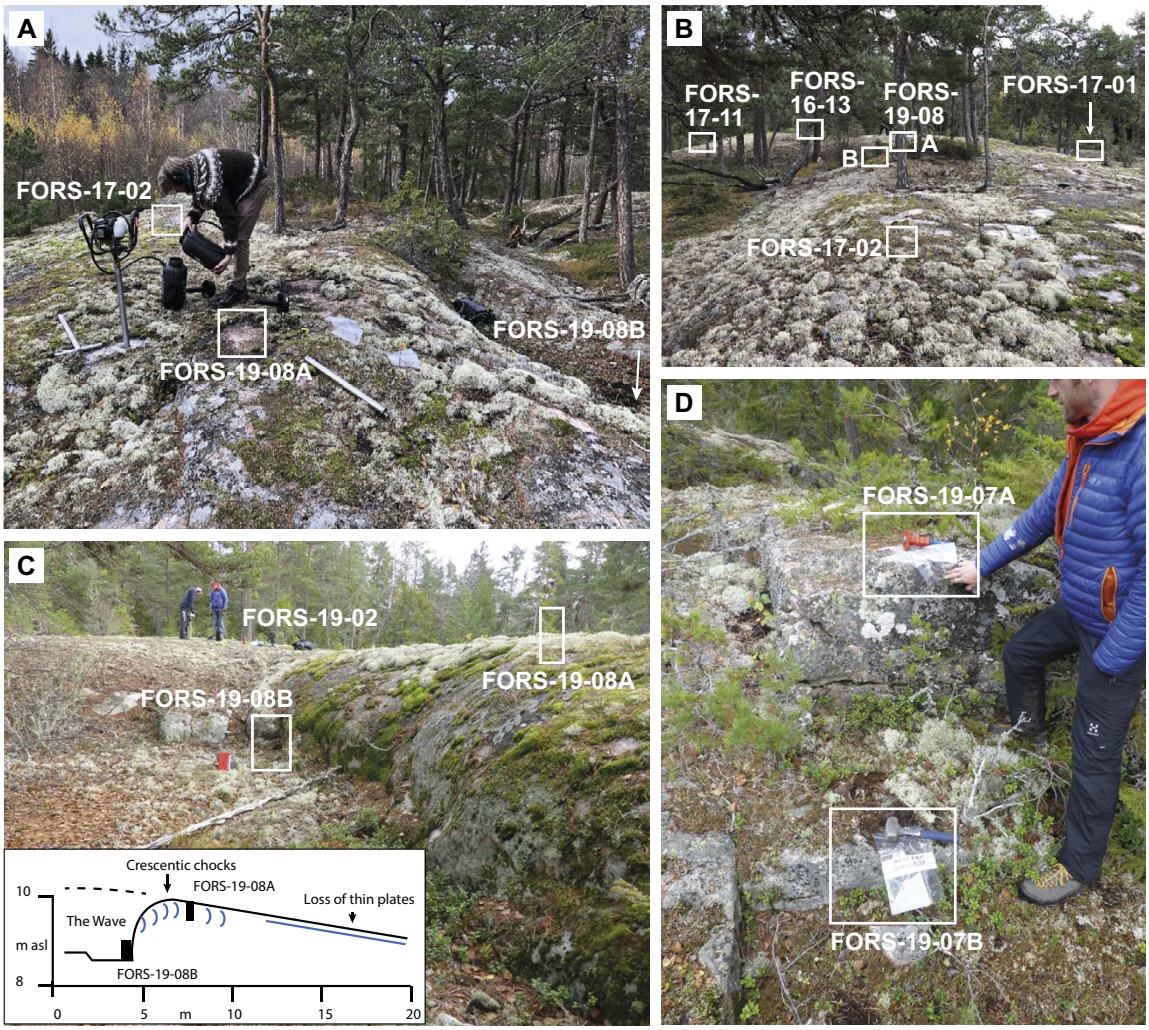

Figure 2-3. *Summit surface samples from Wave Rock. A. View to W along The Wave ridge. B. View to E along The Wave ridge showing TCN sample site locations. C. Detailed view to E of The Wave step (FORS-19-08) with a sketch showing the distribution of micro-erosion forms. Core sample site FORS-19-02 in the background. D. Detailed view of the second step sample site (FORS-19-07) on the eastern side of the outcrop.*

Fractures are more closely spaced on the stoss face of the hill (FORS-17-03) and on the low whalebacks that are found to the south (FORS-17-04 and 17-05). Vertical spacing of curved subhorizontal fractures is 20–30 cm, reaching 50 cm. These sample sites are from abraded surfaces, but adjacent fracture-bounded sockets indicate loss of blocks. The southernmost sample site (FORS-17-05) shows spalling of 5–10 cm thick sheets from the top surface of a low whaleback. Such microforms indicate that the lower, peripheral surfaces have been eroded by combined abrasion and block removal.

2.3.5 Previously sampled coastal sample sites

Samples for cosmogenic isotope analysis were taken from coastal outcrops at Stora Asphällan, Klubbudden, and Stånggrundet in 2016 and 2017. Some samples did not yield reliable TCN data; other sample results are presented in Hall et al. (2019). The sample surfaces are abraded and show damage from late block removal (Figure 2-4), with similar sharp edges, fracture facets, and other microforms to those described for parts of other coastal outcrops in Krabbendam et al. (2023). Each surface shows short, closely spaced (0.1–1.5 m) vertical and horizontal (0.1–0.3 m) fractures at shallow depth that divide the rock surface into small blocks. Downwearing of these rock surfaces during the last and earlier glaciations is interpreted to have involved combined abrasion and block removal.

Figure 2-4. *Examples of rock surfaces sampled for cosmogenic nuclides in 2016 and 2017 at coastal outcrops. A. Stora Asphällan FORS-17-23. B. Stora Asphällan FORS-17-12. C. Stånggrundet FORS-17-19. D. Klubbudden FORS-17-16. White arrows indicate fractures in the shallow subsurface. Blue arrows indicate ice flow direction. Abraded surfaces (a) and sockets (s) are also shown. Samples FORS-17-16 and FORS-17-23 did not yield reliable TCN data.*

2.4 Glacial erosion simulations

Glacial erosion is simulated based on the depth and time dependent production of ^{10}Be and ^{26}Al for a range of scenarios that include different start times for first exposure to TCNs and two contrasting erosion modes yielding various production rates over time for the individual samples. We use the expage glacial erosion calculator version 202306 (http://expage.github.io/calculator; glacialE.m) which is an updated version of the calculator used in Hall et al. (2019). Major parts of the calculator, in particular concerning production rate calculation methods, are based on the original CRONUS calculator (Balco et al. 2008) the Lifton-Sato-Dunai (LSD) production rate scaling code (Lifton et al. 2014) and the CRONUScalc calculator (Marrero et al. 2016). The calculator employs the geomagnetic framework and time steps of Lifton (2016) with the SHA.DIF.14k model (Pavon-Carrasco et al. 2014). The depth dependent ^{10}Be and ^{26}Al production rate from spallation and muons is calculated using the LSD production rate scaling, with reference spallation production rates calibrated based on a global set of calibration data from i) sites with ^{10}Be data and ii) sites with ^{26}Al data, see the expage web site. Time-constant production from muons is calibrated using a modified method of CRONUScalc (Marrero et al. 2016) for ^{10}Be and ^{26}Al data from four deep bedrock cores from Spain, France, and Antarctica (Balco 2017). Weighted averages of the calibration parameters from the four sites are used for the expage calculator. As the calibrated parameters from Beacon Heights have significantly lower uncertainties compared to the other three sites, the weighted parameters are close to the Beacon Heights parameters. Because production by muons affects the calibration of production from spallation and vice versa, the calibration is carried out iteratively for spallation and muons until the parameter values converge (Borchers et al. 2016). This yields a reference ^{10}Be production rate of 4.01 ± 0.25 atoms g^{-1} yr^{-1} and a reference ^{26}Al production rate of 28.31 ± 2.22 atoms g^{-1} yr^{-1}. The site atmospheric pressure is estimated based on the ERA-40 reanalysis (Uppala et al. 2005). The attenuation length, quantifying the reduction in cosmogenic nuclide production from spallation with depth, is determined based on site location and geomagnetic cut-off rigidity using the LSD method as implemented in CRONUScalc (Marrero et al. 2016). This yields an attenuation length of c. 152 g cm^{-2} for the Forsmark region which is somewhat lower, resulting in a more rapid decline in production from spallation with depth, than the commonly used value of 160 g cm^{-2} (Gosse and Phillips 2001, Balco et al. 2008).

Glacial erosion is calculated for two different modes: (1) with continuous glacial erosion rate and (2) with incremental glacial erosion depths. Mode 1 is expressed below as a rate (mm/ka) whereas Mode 2 is expressed as a depth (cm/glaciation). The same calculation was done by Hall et al. (2019). For the case of continuous glacial erosion rate, glacial erosion is assumed to occur continuously during periods with ice cover, and the total amount of erosion scales with the duration of ice cover. For the case of incremental glacial erosion depth, glacial erosion is assumed to occur step-wise only, with cumulative erosion to a constant depth at the end of each ice cover period, and the total depth of erosion scales with the number of ice cover periods. For both modes of erosion, we assume that the glacial erosion is constant through time with either a constant rate of erosion through each ice cover period or a constant depth of erosion for each ice cover period. These assumptions of constant glacial erosion rate during ice cover or constant erosion depth per glacial cycle are crude simplifications that are likely not capturing the complex reality of glacial erosion through time, but are necessary simplifications to enable crucial analysis and quantification of the glacial erosion depths and rates.

The calculation of cosmogenic nuclide production through time is affected by a range of input parameters, including standard cosmogenic nuclide analysis parameters such as sample coordinates, elevation, thickness, density, topographic shielding, and subaerial non-glacial erosion. Additional input data includes the point in time for start of the simulation, ice cover history, and post-glacial submergence under water due to changes in relative sea-level. The point in time for start of the simulation defines the start of cosmogenic nuclide production for the entire bedrock column, implying that before this point in time, the sample must have been shielded from cosmic rays. An implicit assumption of this simulation setup is that at or just before the simulation start point, assuming that it lies recent enough considering the cosmogenic nuclide half-life, there must have been significant erosion to remove all previously produced cosmogenic nuclides.

The ice cover history is determined by the LR04 stack $\delta^{18}O$ record (Lisiecki and Raymo 2005) using a break value at 4.5 ‰ as a best guess for the Forsmark region (Figure 2-5). This yields a record of ice cover during Marine Isotope Stage (MIS) 2 and MIS 4 with ice free conditions during MIS 3, as indicated by proxy data (Alexanderson 2010, Möller et al. 2013, Kleman et al. 2021). Because this break value yields a timing for the last deglaciation that pre-dates the well-constrained timing of deglaciation in the region around 10.8 ka (Stroeven et al. 2016), the ice cover following the Last Glacial Maximum (LGM) is terminated at the time of the interpolated deglaciation based on Stroeven et al. (2016). Because of isostatic and eustatic changes and the low elevation of the region, all samples have been submerged following deglaciation with subsequent isostatic uplift and emergence from water. Production of cosmogenic nuclides while submerged under water is calculated assuming a density of 1.0 g cm^{-3} for water. The water depth is calculated individually for each sample using interpolated parameters for the uplift model of Påsse and Daniels (2015) and modified by a factor of 1.09 based on calibration to ten sites with uplift related isolation levels dated by radiocarbon (Hedenström and Risberg 2003) (Figure 2-6). Currently, we regard this as the most accurate information available to constrain water depths. Brief explanations for the simulation inputs including employed uncertainties are presented in Table 2-1.

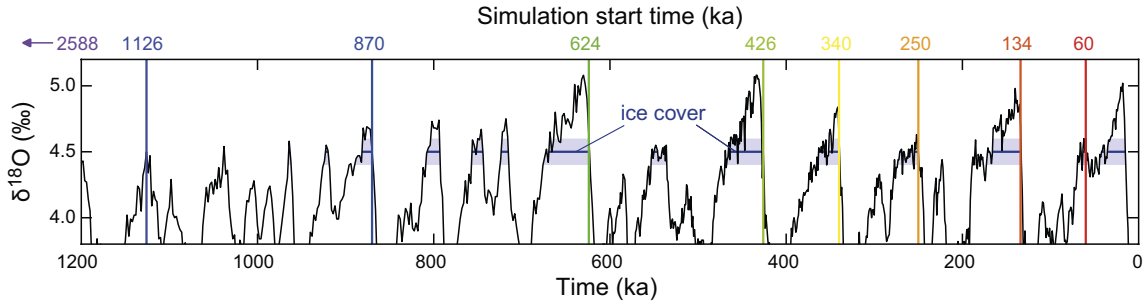

Figure 2-5. *The LR04 benthic $\delta^{18}O$ stack (Lisiecki and Raymo 2005) used to determine the ice cover record for the study site. The site is assumed to have been ice covered for the periods with $\delta^{18}O$ values higher than a break value of 4.5 ‰ with an uncertainty range of 4.4–4.6 ‰ (blue region) The coloured vertical lines display the glacial erosion simulation starting points at the end of the ice cover periods.*

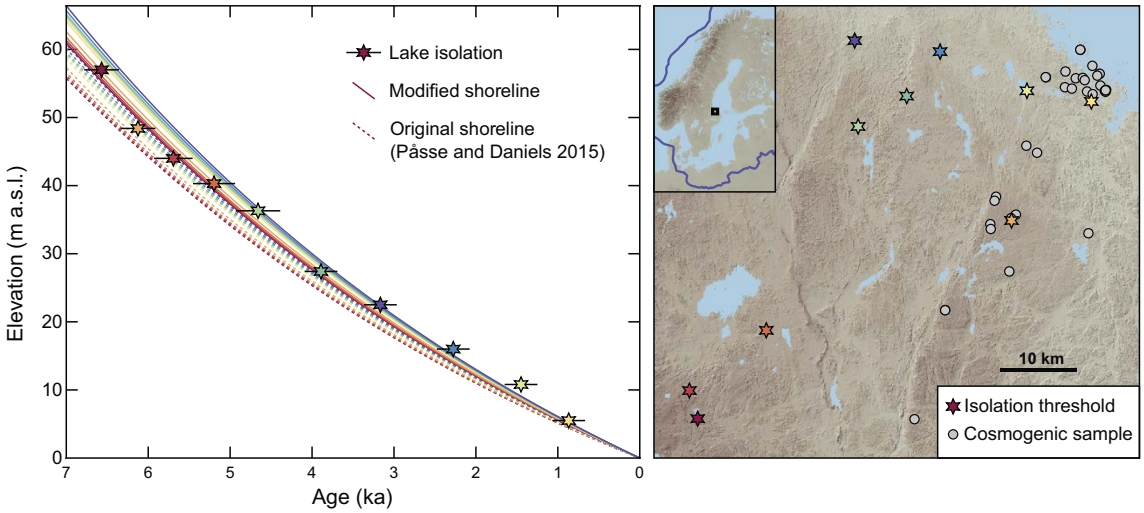

Figure 2-6. *Site-specific original and modified shoreline displacements based on the Påsse and Daniels (2015) model and the lake isolation site elevation and age. The modified shorelines use the Påsse and Daniels (2015) model multiplied by a factor of 1.09 based on calibration to the lake isolation ages and elevations using a weighted mean. The radiocarbon ages have been re-calibrated to the IntCal20 calibration curve. Year zero is 2000 AD. The colours of the lake isolation sites and shoreline curves in the left panel correspond to the colours in the right panel map.*

To calculate the glacial erosion, the end concentration of ^{10}Be and ^{26}Al is calculated for a scenario using the mid-point input parameters for all input variables with uncertainties (Table 2-1) but varying the glacial erosion. The glacial erosion can then be interpolated from the simulated output ^{10}Be and ^{26}Al concentrations, the varied glacial erosion, and the measured sample ^{10}Be and/or ^{26}Al concentration. To estimate the uncertainty of the glacial erosion, the concentration of ^{10}Be and ^{26}Al is simulated in a Monte Carlo method with random generation of the input parameters with uncertainties (Table 2-1) using 10^4 iterations. As the production of cosmogenic nuclides varies non-linearly with varying input parameters, the associated glacial erosion for each individual Monte Carlo iteration is estimated using an iterative approach. With this method, we can find the range of glacial erosion rates that satisfies the measurements for subaerial erosion and ice cover histories. This method also enables calculation of erosion histories for ^{26}Al/^{10}Be pairs as only certain solutions yield a match for both measured nuclide concentrations. For more details, see Hall et al. (2019), Appendix 5.

For the 5 step samples, we first calculate glacial erosion for the top samples. This glacial erosion is then used as input glacial erosion for the full period until the last deglaciation, and we then calculate the depth of glacial erosion during the last ice cover period for the lower sample. Since the paired step samples are from the same site, we expect the lower samples to have experienced identical or close to identical glacial erosion histories to the top samples apart from the glacial erosion (presumably by block removal) creating the step. Hence, assuming that the steps were created by glacial erosion during the last ice cover period, we expect the simulated depth of erosion to conform to the depth of the lower sample. We simulate the glacial erosion based only on the ^{10}Be concentrations, based only on the ^{26}Al concentrations, and on the combined ^{10}Be and ^{26}Al concentrations.

For the single Wave Rock depth profile, we simulate the glacial erosion for each individual sample and calculate a weighted mean glacial erosion using relative sample ^{10}Be and ^{26}Al concentration uncertainties for weighting. This is done with the expage code glacialEdepth.m. We calculate the chi-square P-value for the probability that all sample ^{10}Be or ^{26}Al concentrations can be explained within their uncertainties by the simulation scenario. To evaluate the possibility that one or more of the depth profile samples have erroneous ^{10}Be or ^{26}Al measurements, we run the simulations with samples at various depths excluded to try to get the best match between the simulated and measured ^{10}Be and ^{26}Al concentrations. The samples to exclude were determined based on the ^{10}Be and ^{26}Al concentrations, sample depths, and relation to simulated depth profiles for the full set of samples.

For both the depth profile and the step samples, we simulate the glacial erosion with nine different simulation start times ranging from 2.588 Ma to 60 ka, corresponding to the end of ice cover periods determined by the LR04 record and a $\delta^{18}O$ break value of 4.5 ‰ and the start of the Quaternary period (Figure 2-5). Thus, we use the depth profile and step samples to help determine the simulation start time and thereby the maximum duration back in time for which the cosmogenic nuclides can give any information about past glacial erosion.

Using the glacial erosion simulation scenarios defined by the input parameters (Table 2-1), we simulate the glacial erosion of all new surface samples and all surface samples from Hall et al. (2019). This is done for ^{10}Be alone, ^{26}Al alone, and combined ^{10}Be and ^{26}Al measurements, and for both continuous glacial erosion rate and incremental erosion depth steps.

Table 2-1. Input parameters and uncertainties employed in the glacial erosion simulations.

Parameter	Description	Uncertainty
Sample site coordinates	Latitude and longitude (WGS-84) based on GPS.	No uncertainty used in simulation.
Sample elevation	Based on site coordinates and LiDAR data with 2 m horizontal resolution.	No uncertainty used in simulation.
Sample thickness/depth	Sample thickness is estimated by sampling for surface samples. Sample depth measured for depth profile samples.	No uncertainty used in simulation.
Bedrock density	Bedrock density assumed to be 2.65 g/cm^3.	Assumed to be 0.1 × 2.65 g/cm^3.
Topographic shielding	Estimated based on surface strike and dip.	No uncertainty used in simulation.
Cosmogenic nuclide concentration	Measured using standard AMS methods.	Based on measurements.
Subaerial erosion rate	A constant subaerial erosion rate in the range 0–5 mm/ka, with the mid-point 2.5 mm/ka assumed to be the best guess, is assumed for all ice-free periods when exposed above sea-level.	A uniform distribution of the erosion rate in the range 0–5 mm/ka is used for uncertainty estimation.
Simulation start	The simulation starts at some point in the range 200–1 000 ka, with the mid-point 600 ka assumed to be the best guess. This is based on the paired step samples and the depth profiles.	A uniform distribution of the simulation start time in the range 200–1 000 ka is used for uncertainty estimation.
Ice cover break value	A break value in the range 4.4–4.6 ‰ for the LR04 $\delta^{18}O$ record is used to determine the periods of ice cover. This is based on the $\delta^{18}O$ record for the last glacial cycle.	A uniform distribution of the break value in the range 4.4–4.6 ‰ is used for uncertainty estimation.
Deglaciation	Time of deglaciation interpolated from the Stroeven et al. (2016) reconstruction.	An uncertainty of 500 years is assumed for the deglaciation age.
Postglacial isostatic adjustment	The post-glacial shoreline displacement is interpolated for each sample from the Påsse and Daniels (2015) model and modified by a factor of 1.09. The modification is based on calibration to radiocarbon-dated isolation levels in the region (Hedenström and Risberg 2003) (Figure 2-6).	The elevation adjustment is assumed to have an uncertainty of 10 %.

We generate estimates for glacial erosion rates and incremental erosion depths for the last glaciation (35.4–10.8 ka) to allow comparisons with i) average depths of block removal estimated from mapping of the drone survey sites (Krabbendam et al. 2023), ii) depths of glacial ripping in the Forsmark area (Hall et al. 2020), and iii) long term glacial erosion based on geomorphological criteria (Hall et al. 2019).

We examine spatial variability in the estimated erosion rates by comparing three groups of existing and new bedrock samples:

1. Samples from the summit of Wave Rock (FORS-16-13, 17-01, and 17-11, 19-02A, 19-07A and 19-08A).
2. Samples from the lower ground around Wave Rock (FORS-17-03, 04, and 05).
3. Samples from the coastal outcrops mapped in the drone survey (FORS-17-12 and 17-23 from Stora Asphällan), FORS-19-03A, 19-04 from Lilla Sandgrund), FORS-17-14 and 17-19 from Stånggrundet) and FORS-17-21 (Apelviken, a shallow inlet to the west of Stånggrundet).

The Wave Rock summit surface carries only abrasion forms and the vertical spacing of sheet joints is > 1.14 m. TCN inventories likely constrain abrasion rates through at least the last glaciation. The lower ground around Wave Rock has closer fracture spacings with a mix of microforms indicating combined abrasion and block removal and is more typical of the rock surfaces mapped for coastal outcrops during the drone survey.

3 Results

3.1 Estimation of terrestrial nuclide inheritance

If calculating simple exposure ages, assuming one period with full exposure to cosmic rays, the new samples yield ^{10}Be (^{26}Al) exposure ages ranging from 4.3 ± 0.6 to 49.5 ± 3.6 ka (4.8 ± 0.7 to 49.1 ± 4.5 ka). Six of the samples yield exposure ages up to 13.3 ± 1.1 ka, while the three top samples from the Wave Rock site yield ^{10}Be and ^{26}Al exposure ages in the range 36–49 ka. Taking shielding by water during isostatic uplift into account, the six younger exposure ages are 3.7–7.3 ka older than expected assuming that the bedrock had zero cosmogenic nuclides at the time of the last deglaciation, and the Wave Rock top samples are 34.4–47.6 ka older than expected (Figure 3-1). All samples yielded TCN inventories above those expected for simple deglaciation ages and must include inherited TCNs.

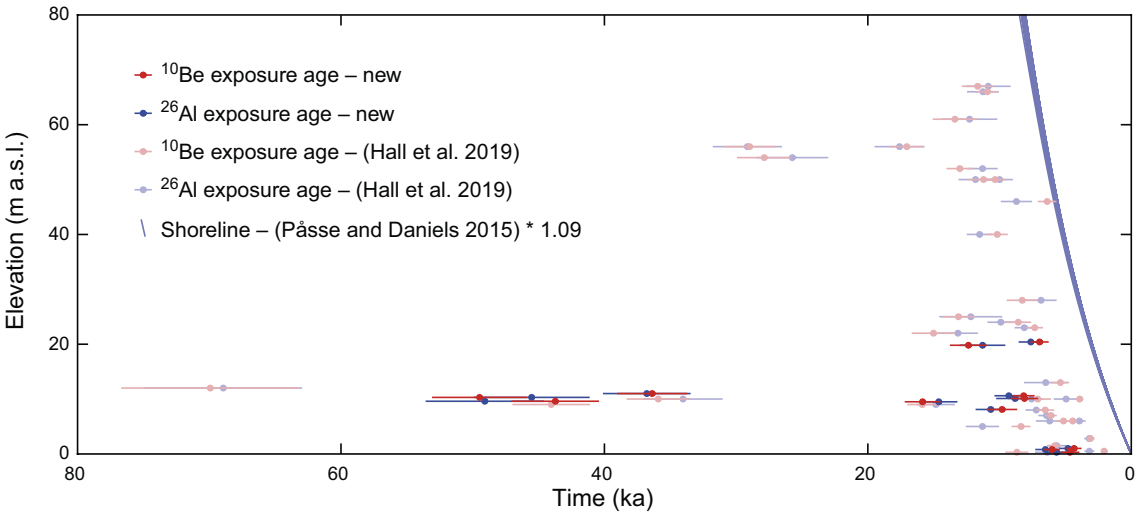

Figure 3-1. *^{10}Be and ^{26}Al exposure ages against sample site elevation and shoreline history. The fact that the samples are significantly older than the associated shoreline age indicates that the samples have experienced cosmogenic nuclide production prior to the last ice cover period implying that the glacial erosion has been limited. The exposure ages of the 11 new samples are similar to the published exposure ages (Hall et al. 2019). As the shoreline history varies spatially, individual shoreline history curves for all 43 sample sites are included. The slight difference in the shoreline histories thereby reflect the spatial difference in isostatic uplift.*

3.2 Bedrock step samples

In the simulations for bedrock step samples, there are various temporal starting points of the simulation. The top sample ^{10}Be (^{26}Al) data yield glacial erosion rates of 8–81 mm/ka (7–70 mm/ka) and incremental glacial erosion steps of 7–86 cm/glaciation (7–76 cm/glaciation) (Figure 3-2). Using these glacial erosion values in the simulation of block removal depth during the last ice-covered period, we derive depths of 0–250 cm compared to the expected step depths of 45–155 cm. For one of the paired step samples (FORS-19-6A/6B – Mohägnaden), the lower sample has a ^{10}Be concentration overlapping with the top sample concentration and an ^{26}Al concentration much higher than expected given the step depth of 60 cm. This shows that the simulation scenario with plucking during the last ice cover period cannot explain the ^{10}Be ^{26}Al concentrations. A simple explanation for this is that the bedrock step was created prior to the last ice-covered period so that both the top sample and the lower sample were exposed to cosmic rays during a pre-Last Glacial Maximum ice-free period. For the remaining four paired step samples, the simulated step depths overlap well with the actual step depths for the simulations starting at 134 ka to 870 ka, indicating that simulation start points after 1 Ma yield best results for the assumption that the bedrock steps were created during the last ice cover period (see 2nd and 4th row in Figure 3-2).

3.3 Wave Rock depth profile

For the depth profile simulations (FORS 19-02-1 to 19-02-6), the ^{10}Be (^{26}Al) data yield glacial erosion of 0–23 mm/ka for constant glacial erosion rates (0–23 mm/ka) or 0–20 cm for constant glacial erosion depths (0–21 cm/glaciation) for the full set of samples (see first row in Figure 3-3). For all simulations with the full set of samples the P-value is 0, indicating that there is either something wrong with the simulation scenario or there is one or more samples with anomalous ^{10}Be and ^{26}Al inventories. We simulated the glacial erosion with single sample 6 with potentially anomalous ^{10}Be inventory excluded, and with single samples 1 and 2 with potentially anomalous ^{26}Al inventories excluded. We also excluded samples 1 and 6 and samples 2 and 6. For these five simulations with one to two samples at different depths excluded, we estimate glacial erosion of 0–25 mm/ka (0–28 mm/ka) or 0–22 cm/glaciation (0–24 cm/glaciation). The ^{10}Be data generally fit better with slightly younger simulation starting points (250–624 ka) compared to the ^{26}Al data (624–2 588 ka). The only simulations yielding P-values > 0.05 for both ^{10}Be and ^{26}Al are with samples 2 and 6 excluded. For both the simulations with constant erosion rates and for the simulations with incremental erosion steps, this is achieved with the simulation start point at 624 ka.

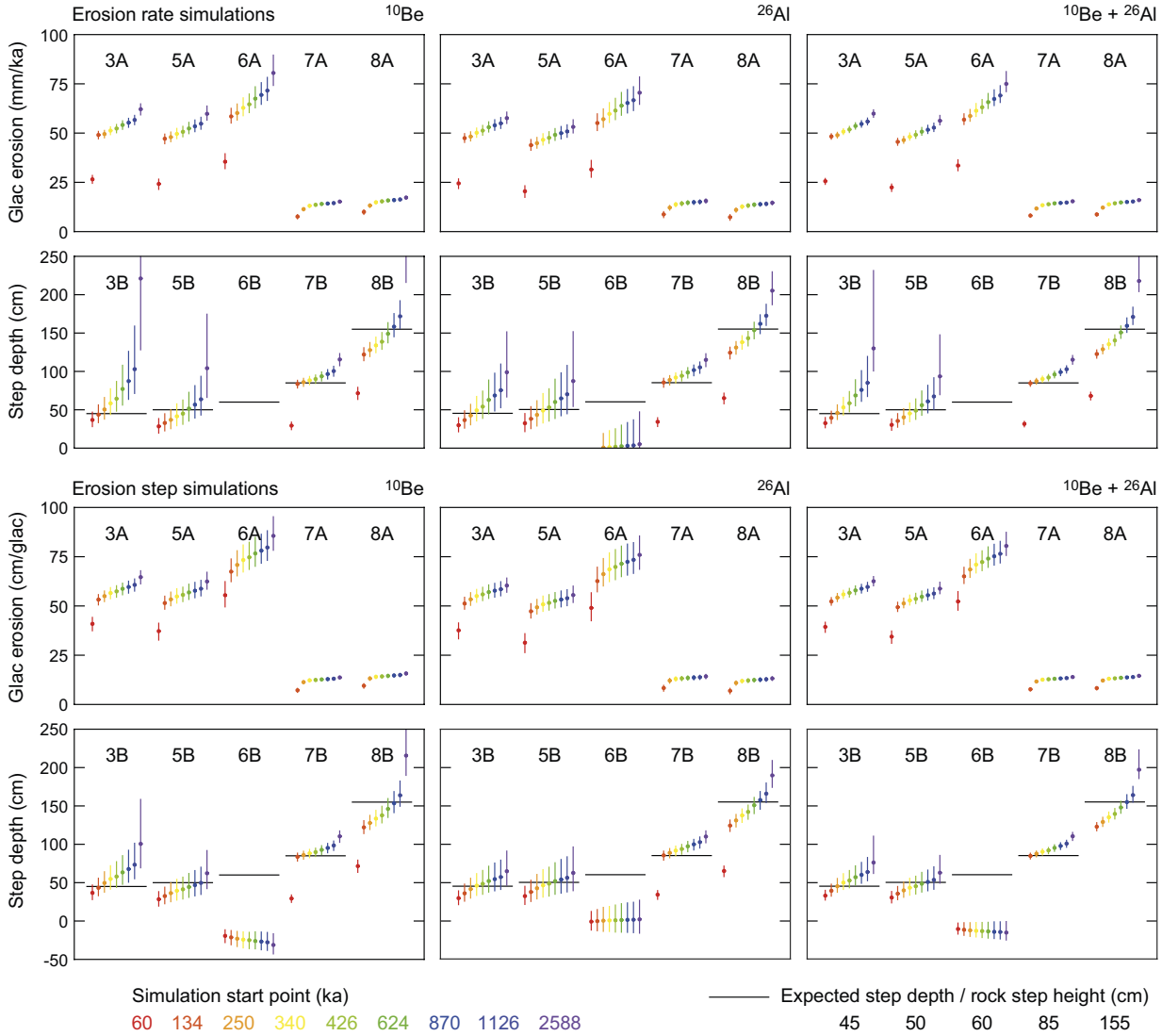

Figure 3-2. *Simulated glacial erosion and associated glacial plucking depth for the five paired rock step samples and for nine different simulation start points (Figure 2-5). The two uppermost rows of panels display results for simulations with constant glacial erosion rates and the two lowermost rows of panels display results for simulations with incremental glacial erosion steps. Panel rows 1 and 3 display the simulated glacial erosion for the surface samples (3A–8A) and panel rows 2 and 4 display the associated simulated step depth during the last deglaciation for the lower samples (3B–8B). The horizontal black lines show the step depth from the top of the rock step to the lower (B) samples. In the erosion step simulations, the simulated step depth (lowermost row of panels) is calculated from the simulated full step depth for the last deglaciation minus the associated glacial erosion depth for the top sample (panel row 3). The negative values for sample 6B indicate that if other parameters of the simulation are correct the lower sample 6B cannot have experienced more glacial erosion during the last ice cover period than the top sample 6A.*

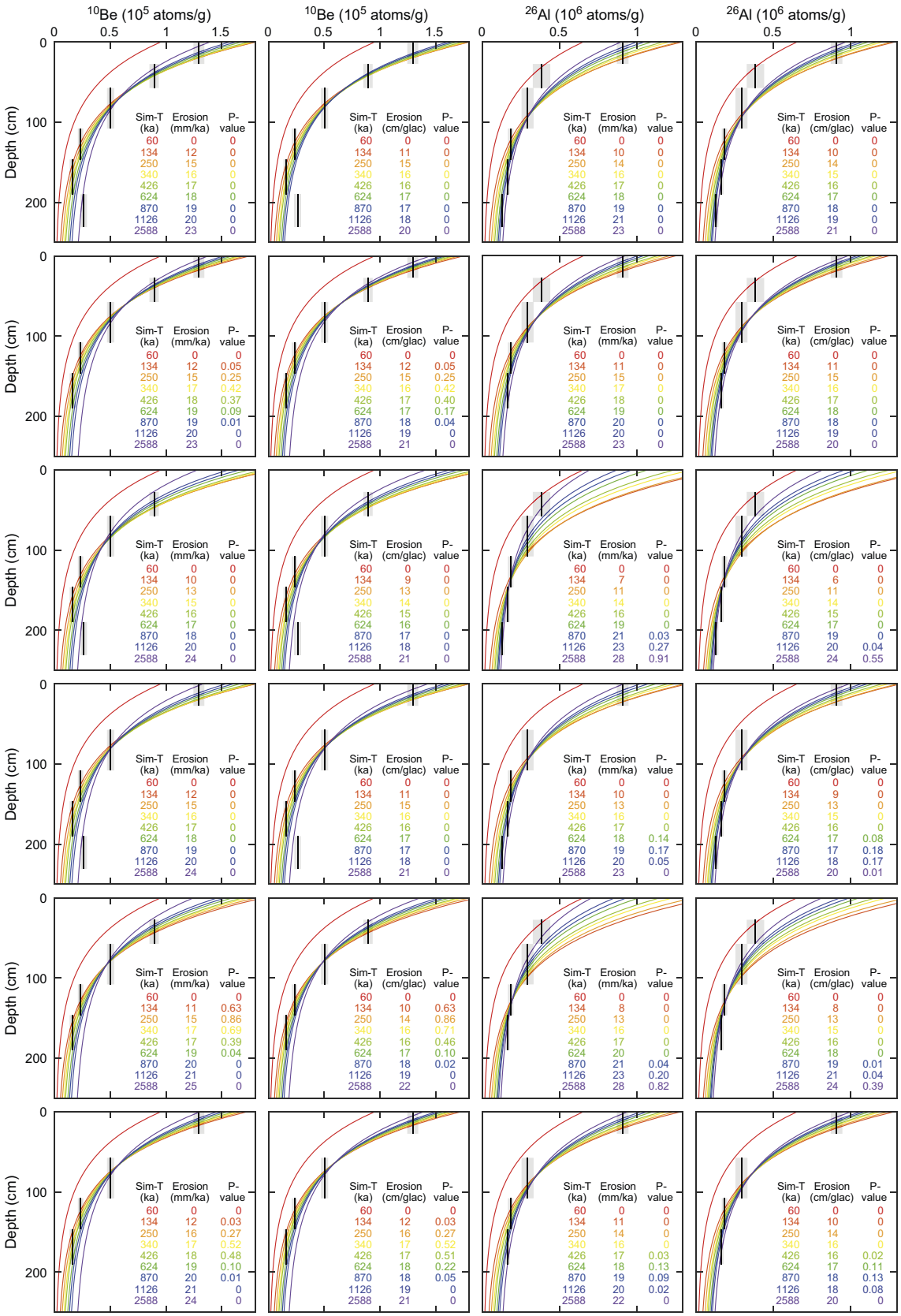

Figure 3-3. *Measured and simulated cosmogenic nuclide concentrations for the depth profile collected from the top of Wave Rock. Columns 1–2 show ^{10}Be concentrations and columns 3–4 show ^{26}Al concentrations. Columns 1 and 3 show simulated depth profiles assuming constant glacial erosion rate. Columns 2 and 4 show simulated depth profiles assuming incremental erosion steps. Each row show data for a specific set of samples with zero, one, or two samples excluded. All simulations were run with start points ranging from 60 ka to 2.588 Ma (Figure 2-5) and display best-fit glacial erosion and associated chi-square P-values for each set of simulated depth profiles. The chi-square P-values are for the hypothesis that the sample concentrations can be explained by the simulation scenario yielding the simulated depth profile.*

3.4 Glacial erosion estimates

Based on the results from the bedrock step sample simulations and the depth profile simulations, we set the simulation starting point to 600 ka and use a uniform uncertainty ranging from 200 ka to 1 Ma for the Monte Carlo uncertainty estimations.

The simulated erosion history of all surface samples from Hall et al. (2019) and this study is shown in Figure 3-4. Individual and summed probability curves of the glacial erosion rates and incremental glacial erosion steps are shown in Figure 3-5. The simulated constant glacial erosion rate for ^{10}Be (^{26}Al) range from 10 (9) to 279 (86) mm/ka, with a weighted mean (Birch and Singh 2014) glacial erosion rate of 53 ± 19 mm/ka (53 ± 17 mm/ka). The simulated incremental glacial erosion steps for ^{10}Be (^{26}Al) range from 8 (8) to 257 (100) cm/glaciation, with a weighted mean glacial erosion of 53 ± 24 cm/glaciation (56 ± 22 cm/glaciation). For the combined ^{10}Be and ^{26}Al simulations, 32 out of 38 samples yield glacial erosion based on ^{10}Be and ^{26}Al that overlap within internal uncertainties (uncertainties based only on ^{10}Be/^{26}Al concentration uncertainty, reference production rate uncertainty, and decay constant uncertainty), for both the constant erosion rate scenario and the incremental erosion step scenario. These combined ^{10}Be and ^{26}Al simulations yield glacial erosion rates ranging from 9 to 87 mm/ka, with a weighted mean glacial erosion rate of 53 ± 17 mm/ka. The combined ^{10}Be and ^{26}Al simulations yield incremental glacial erosion steps ranging from 8 to 102 cm/glaciation, with a weighted mean glacial erosion of 55 ± 22 cm/glaciation.

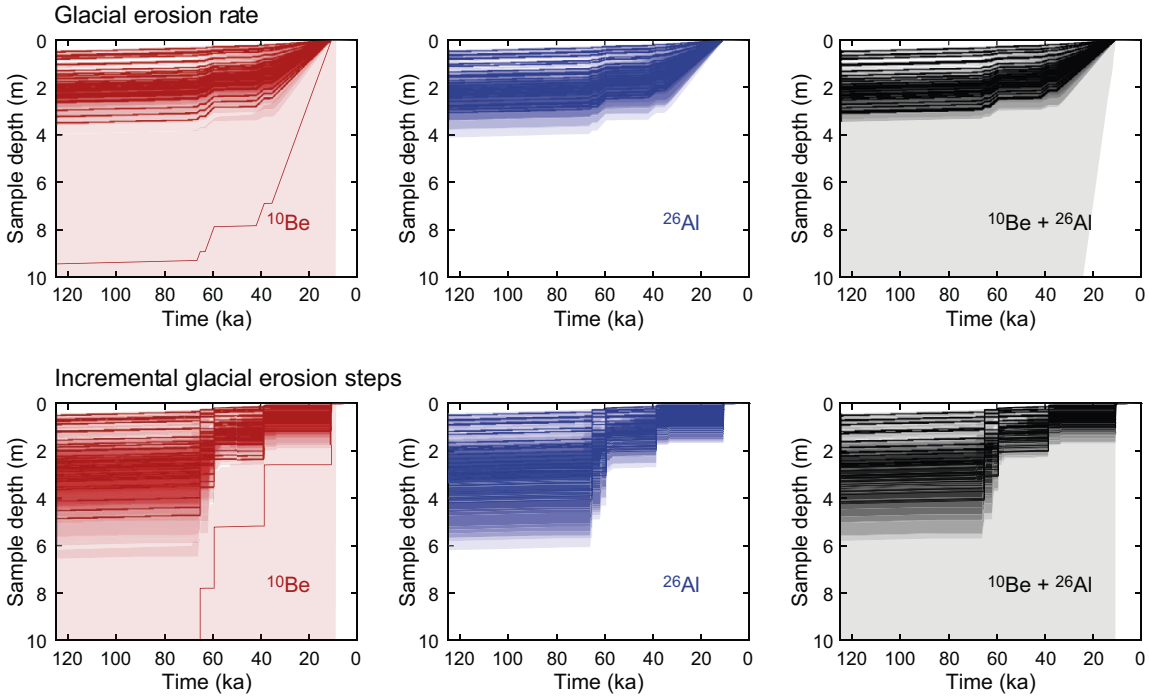

Figure 3-4. *Simulated surface erosion history for all Forsmark bedrock surface samples, i.e. both from the present study and from Hall et al. (2019).*

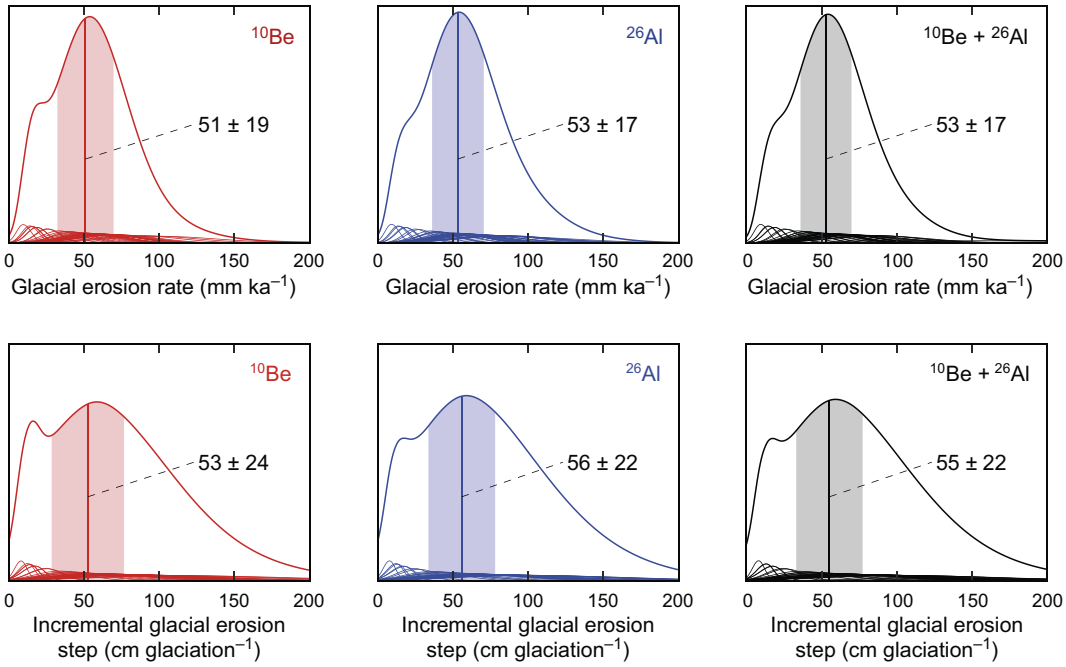

Figure 3-5. *Individual and summed probability density curves of simulated glacial erosion rates (upper row) and incremental glacial erosion steps (lower row) for all Forsmark bedrock surface samples. The vertical lines and shaded areas show the weighted mean glacial erosion rate/step and uncertainty, calculated with the expected value method of Birch and Singh (2014).*

4 Spatial variability of estimated glacial erosion

In this discussion, we explore some of the spatial variability in the TCN inventories and the glacial erosion estimates derived from them in the present study area around Forsmark. We combine the new results reported above with existing results for TCN samples sites from 2016–2018. The contexts of the earlier samples are described in Hall et al. (2019). The locations of all TCN samples are shown in Figure 4-1.

Glacial erosion depths during the last period of ice cover were calculated multiplying the glacial erosion rates for the time period from 35.4 ka BP (when the last ice cover period starts under the scenario using 4.5 per mil for the LR04 record, see Section 2-4) until deglaciation at 10.8 ka (Stroeven et al. 2016). For $^{10}Be/^{26}Al$ nuclides for the 2019 surface samples at Lilla Sandgrund, Gunnarsbo, and Mohägnaden, simulated erosion depths during the last phases of glaciation lie in the range 124–161 cm, close to the weighted mean value of 130 cm for all two-nuclide TCN sample sites in the combined 2016–2019 data. Earlier samples for coastal outcrops yielded the following estimated erosion depths: Stora Asphällan (FORS-17-12: 117 ± 41 cm), Apelviken (FORS-17-21; 215 ± 79 cm), and Stånggrundet (FORS-17-14; 208 ± 73 cm and FORS-17-19; 140 ± 48 cm). Samples FORS-19-7A and 19-8A at Wave Rock (Figure 2-3) yield lower erosion depths of 36–45 ± 14 cm.

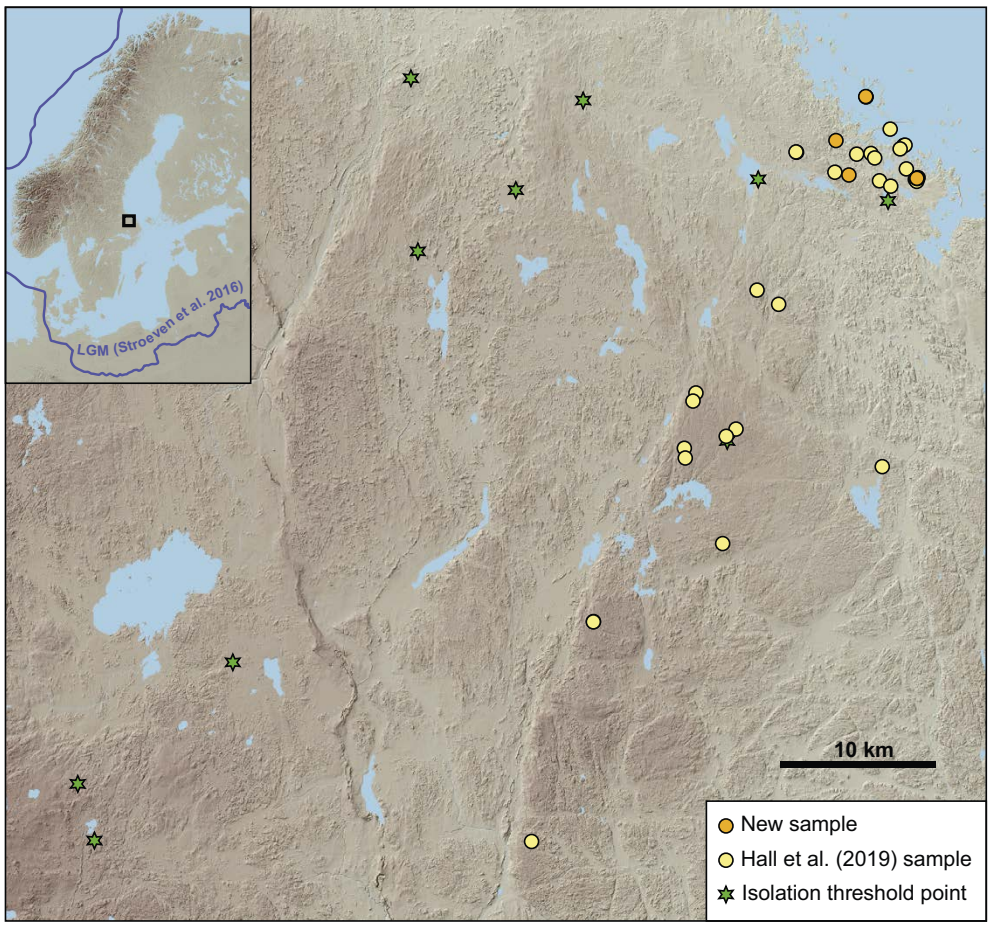

Figure 4-1. *Locations of all cosmogenic nuclide sample sites in the study area and the ten lake isolation threshold points from Hedenström and Risberg (2003) for calibrating the shoreline development model.*

When simulated erosion depths are grouped for the summit surface at Wave Rock, for surrounding lower surfaces at this site and for coastal outcrops, the comparison indicates that the summit surface at Wave Rock experienced significantly lower erosion rates (Figure 4-2). At Wave Rock, the summit surface has erosion depths of 23–46 cm equivalent to erosion rates of 9–19 mm ka^{-1} during the last glaciation. The TCN inventories in the depth profile indicate that erosion rates of 0–22 mm ka^{-1} were likely sustained through several glaciations. Because the smooth summit surface carries microforms from sustained abrasion and not from block removal, we regard erosion through the last glaciation as produced solely by glacial abrasion. This interpretation is supported by erosion depths (23–46 cm) that are significantly less than the > 1.14 m spacing of subhorizontal fractures. Block removal on the hill flanks by plucking has occurred along similarly spaced subhorizontal fractures (Figure 2-3). Estimated erosional downwearing through the last glaciation did not extend down to these fracture depths. Around the base of the hill, the same lithology is more closely fractured, and rock surfaces show microforms indicative of both sustained abrasion and intermittent block removal. Estimated erosion depths are 84–186 cm and equivalent erosion rates are 34–76 mm ka^{-1} for the last glaciation. Erosional downwearing throughout the last glaciation intersected subhorizontal fractures at 20–30 cm spacings. We conclude that combined abrasion and block removal at Wave Rock operated approximately four times faster than abrasion only.

For coastal sites sampled for TCNs (Figures 2-1B and 2-4), fracture patterns are similar to those on low ground around Wave Rock. Glacial micro-forms show that subglacial erosion during deglaciation involved abrasion acting in combination with late block removal. Estimated erosion depths are 117–215 cm and equivalent erosion rates are 47–87 mm ka^{-1} for the last glaciation. Erosional downwearing throughout the last glaciation intersected subhorizontal fractures at 10–30 cm spacings at TCN sample sites (Figure 2-4). Application of the abrasion depths estimated for Wave Rock suggests that combined abrasion and block removal was approximately five times faster than abrasion alone. Abrasion rates however likely varied across the various lithologies of the coastal outcrops and may have been faster than at Wave Rock.

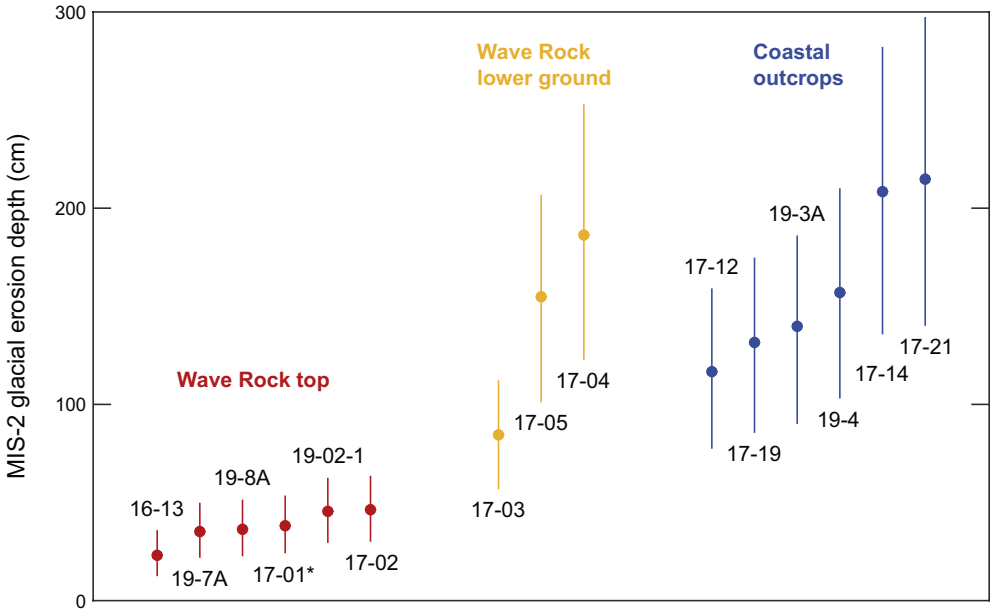

Figure 4-2. *Glacial erosion depths for the last ice cover period for Wave Rock and coastal outcrops. The glacial erosion depth is based on the combined ^{10}Be and ^{26}Al data for surface samples (* for sample 17-01 only ^{10}Be) and the constant glacial erosion rate scenario.*

Glacial erosion through the last glacial cycle at Wave Rock is shown schematically in Figure 4-3. Under the principle of uniformity, rock surfaces with similar fracture patterns and subjected to similar subglacial process can be assumed to erode at similar rates and to develop similar surface forms at a locality. Hence, rock surfaces formed at the terminations of earlier (MIS 4, 6 etc) ice sheet glaciations at Forsmark likely had similar forms to the present surfaces left from the end of the last (MIS 2) glaciation. On the summit surface at Wave Rock, erosion throughout the last glaciation was dominated by abrasion due to the wide spacings of old fractures and the limited development of new, shallow fractures during glaciation. Here, smooth surfaces were maintained by abrasion. On lower surfaces at Wave Rock, and on many other surfaces with higher fracture densities in the Forsmark area, erosion throughout the last glaciation was by combined abrasion and block removal. Prior to ice advance at ~35.4 ka, rock surfaces were probably like today. Islands of abraded surfaces of differing extents, with whaleback and roches moutonnée forms, were bounded by fracture-aligned edges and steps and inset with sockets. On densely fractured rocks, abrasion islands were small and set within extensive low-angle surfaces formed after block removal across subhorizontal fractures. During and after ice advance, the surface roughness of the initial surfaces was first reduced by combined abrasion and intermittent block removal, with further retreat of steps and growth of sockets acting to reduce and, locally, to eliminate the abrasion islands. Later, sustained abrasion beneath thick, sliding ice for a long period around the time of the Last Glacial Maximum led to extensive smoothing across rock surfaces with different fracture densities. During final deglaciation, ice thinned, and large volumes of meltwater were supplied to the bed, triggering a late phase of extensive block removal. The TCN erosion depth estimates do not include this late phase because the TCN samples were taken from abraded surfaces above and between any sockets left by late block removal.

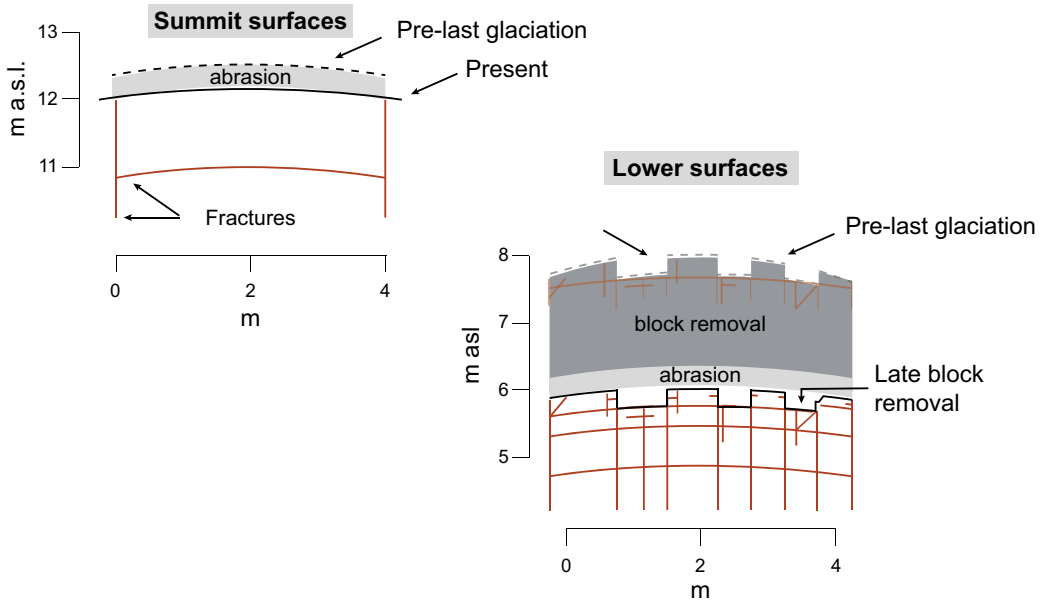

Figure 4-3. *Schematic model of inferred glacial erosion on the summit and lower surfaces at Wave Rock throughout the last glaciation.*

5 Conclusions

Terrestrial cosmogenic nuclide results for samples collected in 2019 add significant new data but are similar to the cosmogenic nuclide results presented in Hall et al. (2019). In line with earlier TCN samples, all the 2019 samples have inherited cosmogenic nuclides produced prior to the last ice cover period showing that depths of glacial erosion were insufficient to remove existing TCNs. Paired samples at 4 rock steps from which blocks have been removed are consistent with block removal during the last ice cover period for simulations starting at 134 ka to 870 ka. The glacial erosion estimates reported here conform with depths and rates reported in Hall et al. (2019) but tend towards the lower end of previous erosion estimates mainly due to the shorter duration of potential cosmogenic nuclide production (later simulation start point). Coastal rock outcrops and low elevation rock surfaces at Wave Rock have relatively high fracture densities and carry glacial microforms indicating erosion by combined abrasion and block removal; glacial erosion depth estimates for the last glaciation between 35.4 ka BP and 10.8 ka are 84–215 cm. Summit rock surfaces at Wave Rock have low fracture densities and carry only abrasion microforms; glacial erosion depth estimates for the last glaciation are 23–46 cm and are interpreted to represent abrasion only. Combined abrasion and block removal operated approximately four to five times faster than abrasion only over the last glaciation in the Forsmark area.

Contributions

The study was initiated by Jens-Ove Näslund (SKB) and it was jointly designed by Jens-Ove Näslund and Adrian Hall (initially at Stockholm University, now at Edinburgh University). Adrian Hall co-ordinated the scientific work on the study and provided descriptions of surface forms and fracturing at the cosmogenic nuclide sample sites. Adrian Hall and Andy Hein (Edinburgh University) collected the samples. Andy Hein carried out the initial sample processing. Jakob Heyman was responsible for cosmogenic data handling, data presentation, and modelling of cosmogenic nuclide erosion and burial histories. Adrian Hall drafted the report; all authors contributed to the final revision of the report. The report was scientifically reviewed by Annina Margreth (Geological Survey of Norway).

References

SKB's (Svensk Kärnbränslehantering AB) publications can be found at www.skb.com/publications.

Alexanderson H, 2010. Sub-till glaciofluvial sediments at Hultsfred, South Swedish Upland. GFF 132, 153–159. https://doi.org/10.1080/11035897.2010.508134

Balco G, 2017. Production rate calculations for cosmic-ray-muon-produced ^{10}Be and ^{26}Al benchmarked against geological calibration data. Quaternary Geochronology 39, 150–173.

Balco G, Stone J O, Lifton N A, Dunai T J, 2008. A complete and easily accessible means of calculating surface exposure ages or erosion rates from ^{10}Be and ^{26}Al measurements. Quaternary Geochronology 3, 174–195.

Bierman P R, Caffee M W, Davis P T, Marsella K, Pavich M, Colgan P, Mickelson D, Larsen J, 2002. Rates and timing of earth surface processes from in situ-produced cosmogenic Be-10. Reviews in Mineralogy and Geochemistry 50, 147–205.

Birch M, Singh B, 2014. Method of best representation for averages in data evaluation. Nuclear Data Sheets 120, 106–108.

Borchers B, Marrero S, Balco G, Caffee M, Goehring B, Lifton N, Nishiizumi K, Phillips F, Schaefer J, Stone J, 2016. Geological calibration of spallation production rates in the CRONUS-Earth project. Quaternary Geochronology 31, 188–198.

Gosse J C, Phillips F M, 2001. Terrestrial in situ cosmogenic nuclides: theory and application. Quaternary Science Reviews 20, 1475–1560.

Hall A M, Ebert K, Goodfellow B W, Hättestrand, C, Heyman J, Krabbendam M, Moon S, Stroeven A P, 2019. Past and future impact of glacial erosion in Forsmark and Uppland. SKB TR-19-07, Svensk Kärnbränslehantering AB.

Hall A M, Krabbendam M, van Boeckel M, Goodfellow B W, Hättestrand C, Heyman J, Palamakumbura R N, Stroeven A P, Näslund J-O, 2020. Glacial ripping: geomorphological evidence from Sweden for a new process of glacial erosion. Geografiska Annaler: Series A, Physical Geography 102, 333–353. https://doi.org/10.1080/04353676.2020.1774244

Hedenström A, Risberg J, 2003. Shore displacement in northern Uppland during the last 6 500 calendar years. SKB TR-03-17, Svensk Kärnbränslehantering AB.

Kleman J, Hättestrand M, Borgström I, Fabel D, Preusser F, 2021. Age and duration of a MIS 3 interstadial in the Fennoscandian Ice Sheet core area – Implications for ice sheet dynamics. Quaternary Science Reviews 264, 107011. https://doi.org/10.1016/j.quascirev.2021.107011

Kohl C, Nishiizumi K, 1992. Chemical isolation of quartz for measurement of in situ-produced cosmogenic nuclides. Geochimica et Cosmochimica Acta 56, 3583–3587.

Krabbendam M, Hall A M, Palamakumbura R M, Finlayson A, 2022. Glaciotectonic disintegration of roches moutonnées during glacial ripping in east Sweden. Geografiska Annaler: Series A, Physical Geography 104, 35–56. https://doi.org/10.1080/04353676.2021.2022356

Krabbendam M, Finlayson A, Palamakumbura R, Hall A M, 2023. Quantifying the contribution of abrasion versus block removal to subglacial erosion on basement rocks. Very-high resolution DSM analysis Forsmark, east Sweden. SKB TR-23-27, Svensk Kärnbränslehantering AB.

Lifton N, 2016. Implications of two Holocene time-dependent geomagnetic models for cosmogenic nuclide production rate scaling. Earth and Planetary Science Letters 433, 257–268.

Lifton N, Sato T, Dunai T J, 2014. Scaling in situ cosmogenic nuclide production rates using analytical approximations to atmospheric cosmic-ray fluxes. Earth and Planetary Science Letters 386, 149–160.

Lisiecki L E, Raymo M E, 2005. A Pliocene-Pleistocene stack of 57 globally distributed benthic δ^{18}O records. Paleoceanography 20, PA1003. https://doi.org/10.1029/2004PA001071

Margreth A, Gosse J, Dyke A, 2014. Constraining the timing of last glacial plucking of tors on Cumberland Peninsula, Baffin Island, Eastern Canadian Arctic. Geophysical Research Abstracts 16, EGU2014-9043.

Marrero S M, Phillips F M, Borchers B, Lifton N, Aumer R, Balco G, 2016. Cosmogenic nuclide systematics and the CRONUScalc program. Quaternary Geochronology 31, 160–187.

Möller P, Anjar J, Murray A S, 2013. An OSL□dated sediment sequence at Idre, west□central Sweden, indicates ice□free conditions in MIS 3. Boreas 42, 25–42.

Nishiizumi K, 2004. Preparation of ^{26}Al AMS standards. Nuclear Instruments and Methods in Physics Research Section B: Beam Interactions with Materials and Atoms 223, 388–392.

Nishiizumi K, Imamura M, Caffee M W, Southon J R, Finkel R C, McAninch J, 2007. Absolute calibration of 10Be AMS standards. Nuclear Instruments and Methods in Physics Research Section B: Beam Interactions with Materials and Atoms 258, 403–413.

Pavon-Carrasco F J, Osete M L, Miquel Torta J, De Santis A, 2014. SHA. DIF. 14k: a new archaeomagnetic model for the Holocene period. Earth and Planetary Science Letters 388, 98–109.

Phillips W M, Hall A M, Mottram R, Fifield K, Sugden D E, 2006. Cosmogenic ^{10}Be and ^{26}Al exposure ages of tors and erratics, Cairngorm Mountains, Scotland: Timescales for the development of a classic landscape of selective linear glacial erosion. Geomorphology 73**,** 222–245. https://doi.org/10.1016/j.geomorph.2005.06.009

Påsse T, Daniels J, 2015. Past shore-level and sea-level displacements. SGU Rapporter och meddelanden 137, Sveriges geologiska undersökning.

SKB, 2020. Post-closure safety for the final repository for spent nuclear fuel at Forsmark. Climate and climate-related issues, PSAR version. SKB TR-20-12, Svensk Kärnbränslehantering AB.

Stephens M B, 2010. Forsmark site investigation. Bedrock geology – overview and excursion guide. SKB R-10-04, Svensk Kärnbränslehantering AB.

Stroeven A P, Hättestrand C, Kleman J, Heyman J, Fabel D, Fredin O, Goodfellow B W, Harbor J M, Jansen J D, Olsen L, Caffee M W, Fink D, Lundqvist J, Rosqvist G C, Strömberg B, Jansson K N, 2016. Deglaciation of Fennoscandia. Quaternary Science Reviews 147, 91–121. https://doi.org/10.1016/j.quascirev.2015.09.016

Uppala S M, Kållberg P, Simmons A J, Andrae U, Bechtold V D C, Fiorino M, Gibson J, Haseler J, Hernandez A, Kelly G, Li X, Onogi K, Saarinen S, Sokka N, Allan R P, Andersson E, Arpe K, Balmaseda M A, Beljaars, Van De Berg L, Bidlot J, Borsmann N, Caires S, Chavalier F, Dethof A, Dragosavac M, Fisher M, Fuentes M, Hagemann S, Hólm E, Hoskins B J, Isaksen L, Janssen P A E, Jenne R, Mcnally A P, Mahfouf J-F, Morcette J-J, Rayner N A, Saunders R W, Simon P, Sterl A, Trenberth K E, Untch A, Vasiljevic, Vinterbo P, Wollen J, 2005. The ERA□40 re□ analysis. Quarterly Journal of the Royal Meteorological Society: A journal of the atmospheric sciences, applied meteorology and physical oceanography 131, 2961–3012.

Xu S, Freeman S P, Sanderson D, Shanks R P, Wilcken K M, 2013. Cl can interfere with Al3+ AMS but B need not matter to Be measurement. Nuclear Instruments and Methods in Physics Research Section B: Beam Interactions with Materials and Atoms 294, 403–405.

Xu S, Freeman S P, Rood D H, Shanks R P, 2014. ^{26}Al interferences in accelerator mass spectrometry measurements. Nuclear Instruments and Methods in Physics Research Section B: Beam Interactions with Materials and Atoms 333, 42–45.

Arkitektkopia AB, Bromma, 2023

SKB is responsible for managing spent nuclear fuel and radioactive waste produced by the Swedish nuclear power plants such that man and the environment are protected in the near and distant future.

skb.se